The Pursuit of Practical Applications of THz CMOS Chips

(Invited)

Ruonan Han

Massachusetts Institute of Technology

Abstract

The deficiency and slow adoption of terahertz (THz) applications have been long attributed to the expensive and under-performing hardware. That has motivated the research of THz CMOS circuits for over 15 years. However, traditional THz applications for astronomy, security screening and material analytics are arguably not a good match to CMOS, which is more suited for large-volume productions. And albeit the large progress of CMOS THz circuit, it is still not attractive enough for its large-volume and most-anticipated application – "*Beyond-5G*" broadband wireless. Aiming to tackle the above dilemma, in this paper we present our approaches that change the focus from "*how CMOS helps making a better THz system*" to "*how THz helps making a better CMOS system*". The demonstrated prototypes include high-resolution radar imager, molecular clock, dielectric wireline link, THz-ID, among others, which showcase the opportunities in applying the combination of THz and CMOS technologies in traditional applications of electronics.

Introduction

While much of the properties of the terahertz (THz) wave have been well studied, the applications of THz band, even of just the lower side of it at 0.1~1THz, was never extensive. As of now, although numerous studies and demonstrations regarding THz new applications have been reported, the wave in practice is only utilized in radio astronomy (with a recent well-known example of blackhole imaging) and niche benchtop imaging/spectroscopic equipment. Many believed that such dilemma is attributed to the lack of more accessible and integrated hardware. Such deficiency motivated the research and development of THz CMOS circuits. Since its debut in ~2008, THz CMOS circuits have made remarkable progress. The radiated power at a few hundred gigahertz has increased from tens of nW [1] to a few mW [2], and almost all common circuit blocks and many chip-scale systems have been implemented. However, the long-expected commercialization of THz CMOS ICs did not gain much momentum. After all, the relatively small production volume of analytical instruments could not much benefit from the cost advantage of CMOS, III-V semiconductor chips are probably a better alternative.

Over the past decade, the adoption of millimeter wave (mmWave) in 5G standards motivated the society to investigate the THz band for "*Beyond-5G*" broadband wireless communications. This passion was further fueled by FCC's decision in opening the 95GHz~3THz spectrum in 2019. Point-to-point links were initially demonstrated using electro-photonic and discrete III-V semiconductor devices, but then soon silicon-based THz wireless transceivers with ~100Gbps data rate were reported [3], [4]. These chip prototypes, however, demonstrate only a few cm to ~1 meter transmission distance and require precise alignment. The corresponding applications are not only limited, but also seem to better suit using free-space laser approaches. They also have not provided competitive energy efficiency, which is critical for mobile scenarios.

The above efforts all aim at a goal of replacing the bulky and costly THz hardware with CMOS chips, in order to better enable the existing THz applications. This goal should be re-examined. First, as some early investigators of THz technologies have pointed out [5], the practicality of those existing applications, and/or the corresponding hardware setup, are questionable. So even the cost and performance bottlenecks are addressed, they may still not compete well with their RF or optical counterparts and gain the critical mass. Second, the interplay between CMOS and THz technologies does not have to be unilateral: in addition to pursue "*how CMOS helps making a better THz system*", we should also explore "*how THz helps making a better CMOS system*", which may target at traditional applications of electronics. Third, we should search for applications which were previously non-existent or impractical in both the traditional electronics and THz regimes but start to make sense when using chip-scale THz systems. To showcase some preliminary efforts following these thoughts, in this paper, some recent work by the MIT's THz integrated electronics team and their collaborators are presented.

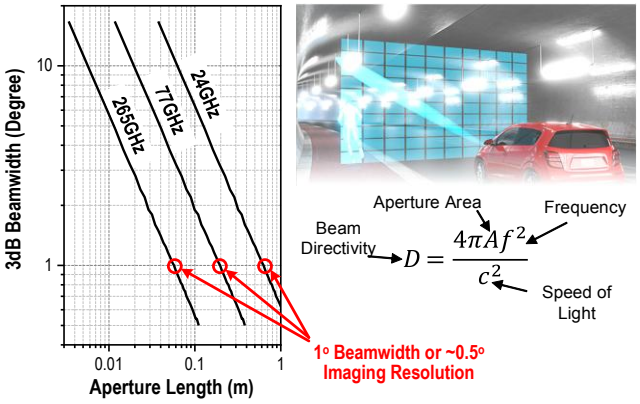

Fig. 1. Beamwidth at varying aperture size and frequency [11]. The imaging resolution is roughly half of the beamwidth due to the double beam sharpening in the TX and RX paths.

THz Imaging: High Resolution, and No More Mechanics

Most THz imaging demonstrations, targeting at revealing the internal of non-metallic objects, are based on a transmission-mode setup where the transmitter (TX) and receiver (RX) are located on the two sides of the objects. They also mostly rely on slow mechanical raster scan of the focused THz spot on the object, in order to generate high lateral resolution images. Such a configuration, while applicable for analytics instruments, does not allow rapid imaging of remote objects, which favors operations in reflection mode and the elimination of mechanical scanners. One solution to the latter is large-scale (>1k pixels) focal-plane sensor arrays, which are so far only implemented at ~1THz and above using microbolometers, CMOS square-law detectors [6], etc. due to the small pixel size at such frequencies. CMOS square-law detector, however, has poor sensitivity (noise equivalent power NEP>1pW/Hz$^{1/2}$) therefore cannot support the desired reflection mode, which requires much higher link budget than the transmission mode does.

Compared to its RF/mmWave counterparts, the THz wave does not offer fundamentally different properties other than its smaller wavelength (hence potentially higher resolution), so the mmWave beam-forming-based imaging radar techniques, which meet the above requirements and are currently under extensive development for autonomous vehicles, can be applied to the THz band as well. More importantly, electronic beam forming at THz offer an interesting alternative solution to the ultimate goal of autonomous vehicle radars — matching the imaging angular resolution of LiDARs. To that end, we note that all radars are limited by the equation in Fig. 1, where the echo-based imaging angular resolution is about half of the 3dB beamwidth. To achieve 0.5° angular resolution in imaging, the aperture dimension required at the mainstream radar frequency of 77GHz is as large as ~20cm but is reduced to only ~6cm at 265GHz (a frequency we conveniently chose due to our available testing instrument). This credit-card size not only makes the fitting of the component behind the bumper or windshield easier, but also makes the filling of the aperture using a dense, phase-shifting antenna array more practical. At 77GHz and below, the large physical aperture size is mostly realized using sparse MIMO arrays which heavily rely on high-precision signal AD conversion and processing of many transceiver channels. With all the above considerations, a sub-THz beam-forming radar may provide LiDAR-grade resolution while still keeping a relatively compact form factor. It is also noteworthy that the mmWave radar's advantage of all-weather reliability still holds for those operating within the 200-to-300GHz window. Experimental studies have shown that in this window, the loss of wave transmission under cloudy, dusty and humid conditions is still low: e.g. 10dB/km under 50% humidity [7]–[10].

2024 IEEE Custom Integrated Circuits Conference (CICC) | 979-8-3503-9406-1/24/$31.00 ©2024 IEEE | DOI: 10.1109/CICC60959.2024.10529072

979-8-3503-9406-1/24/$31.00 ©2024 IEEE

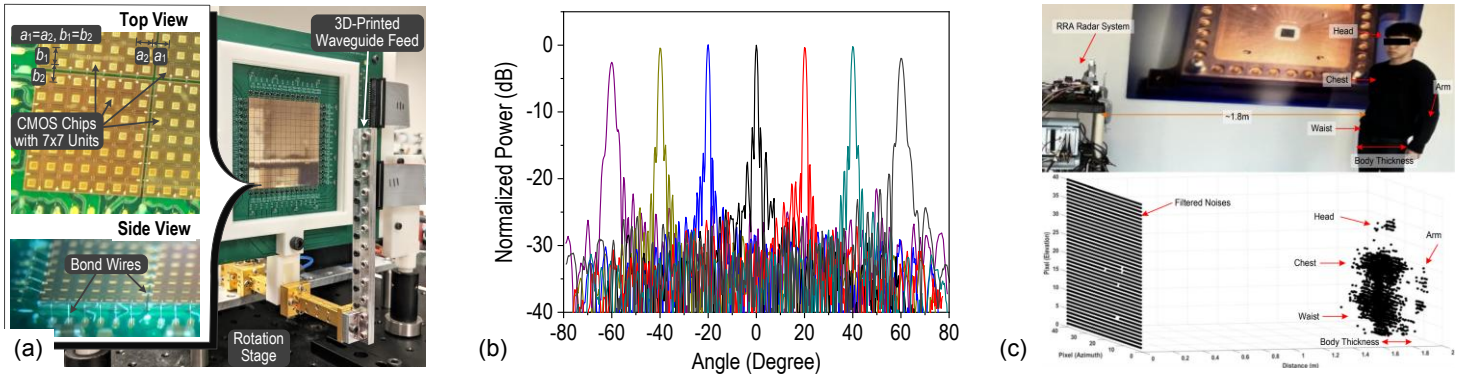

Fig. 2. A 98x98 CMOS reflectarray at 260GHz [11]: (a) tiled CMOS chips that are stitched via bond wires, (b) measured electronic 2D beam forming patterns (different colors correspond to different digital settings) with minimum of 1° beamwidth, and (c) 3D imaging result without relying on any mechanical scanner.

In [11], a 265GHz CMOS reflectarray with 98x98 elements was reported as a result of collaboration between the MIT team and Intel's advanced packaging team. The reflectarray is built with 14x14 tiled chips, each consisting of 7x7 on-chip square patch antennas. The system (Fig. 2a), with a total aperture size of 5.6x5.6cm^2, targets at 1° electronic beam forming. In Fig. 2a, the patch receives incident radiation with *x*- polarization and then routes the signal, through a pair of FinFET switches, to one of the opposite patch edges in the *y*-direction, so that eventually the wave is re-radiated with a cross-polarization. Such a configuration allows for the re-use of the patch antenna for signal backscattering and reduces the interference between the input and output. More importantly, the phase of the reflected wave is controlled by a 1bit digital control (0° or 180°) with phase-independent insertion loss. When pairing with an external sub-THz source (or transceiver for bi-directional TX-RX operation of the reflectarray), the system performs local phase shifting to a diverging illumination and then collimate and steer the beam towards any arbitrary direction. Utilizing the large integration of the CMOS chips, the reflectarray also equips with 80kb of memory under each antenna, so that the pre-calculated control bits associated with each beam direction can be stored and loaded locally during imaging scan, allowing for only <1W of DC power for the whole array. The redundant memory for each beam direction is also used for beam-shape-improvement algorithms, including (1) dithering which scrambles and averages out the 1bit quantization error of beam patterns over time, and (2) squint correction which reduces beam tilting during a broadband FMCW chirp. Note that all these features are not possible in conventional, non-CMOS reflectarrays.

As expected from Fig. 1, the reflectarray forms a 1°-wide beam in the experiment and performs electronic beam steering over >120° of field-of-view in both the elevation (Fig. 2b) and azimuth directions. Based on this system, high-angular-resolution THz imaging without mechanical scanning is demonstrated for the first time. As an example, Fig. 2c shows the 3D surface contour of a human body derived from a reflection-mode setup.

Thanks to the sharp radiation pattern in Fig. 2b, the corresponding beam directivity is as large as 42dBi. That, however, is not translated to an excellent overall radar link budget as one may expect. The problem lies within the on-chip patch antenna, which only provides 12% radiation efficiency (if antenna feed lines are included), or 9dB of insertion loss. Note that in a radar transceiver pairing with the reflectarray, a radar echo signal bounced twice at the on-chip antennas undergoes 4x9dB=36dB of overall loss. This could be addressed by implementing the antennas within the chip package, for which the MIT and Intel teams have previously reported high-performance in-package components at sub-THz frequencies [12]. Our simulation has shown that the radiation efficiency of a 265GHz antenna-in-package (AiP) reaches ~80% (or 1dB insertion loss), thanks to the larger layer thickness and inter-layer distance of in-package metal interconnects. That will dramatically increase the overall radar link budget by 4x(9-1)=32dB. That improvement should allow for the detection of an object with RCS=0.3m^2 at a distance of over 100m, if a CMOS transceiver with 3dBm output power and 12dB noise figure (NF) is used. The AiP, along with chiplet integration technologies for the sub-THz phase shifters, will also reduce the overall consumed silicon area by ~10x, compared to the one in Fig. 2a.

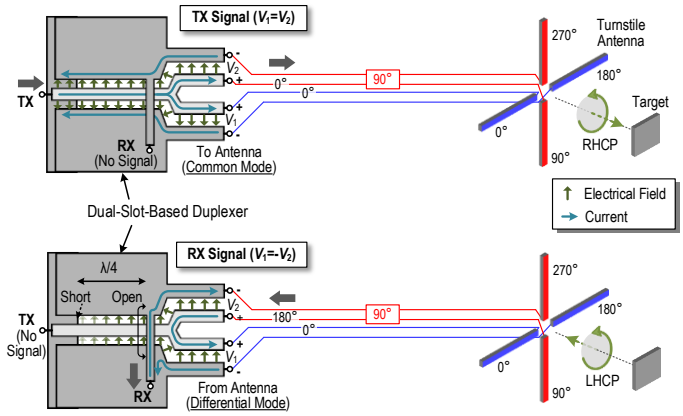

Fig. 3. A mode-based radar duplexing scheme allowing for TX-RX antenna sharing without intrinsic insertion loss [13].

To realize a "full-silicon" imaging system, a sub-THz CMOS radar transceiver is needed to pair with the above reflectarray. To avoid TX-to-RX interference, FMCW radar transceivers normally adopt a bi-static configuration where separate TX and RX antennas are used. However, this causes misalignment between the TX and RX beams [13]; the misalignment angle α normalized to the beamwidth B_m can be estimated as $(d/\lambda)/(F/D)$, where d/λ is the ratio between TX-RX distance and wavelength, and F/D is the ratio between the reflectarray focal length and dimension. For small radar volume, F/D should be kept low due to the inevitably large D in the high-angular-resolution radars. But even for practical values of d/λ=1 and F/D=1, the TX-RX misalignment α is still close to B_m, leading to imaging resolution degradation and 6dB of signal round-trip loss [13]. Co-located or shared TX-RX antenna, therefore, is highly preferred. This typically is achieved using a directional coupler, which inevitably introduces 6-dB insertion loss to the link budget. To avoid such loss, we present a duplexing scheme in [13]. Illustrated in Fig. 3, a pair of orthogonally oriented dipole antennas is driven by two feeds V_1 and V_2, and a 90° passive shifter is inserted in the V_2 path. In the TX mode, V_1 and V_2 are in *common* mode, which generates a right-handed circular polarization (RHCP) wave from the antenna. After the reflection from the object, the wave polarization becomes left-handed; when passing through the antenna and feed network again, the RX signal presents as the *differential* component between V_1 and V_2, which can then be separated from the TX signal using, for example, a dual-slot on-chip structure shown in Fig. 3. As a proof-of-concept of this scheme, a 140GHz CMOS radar transceiver is constructed, which fully eliminates TX-RX misalignment when

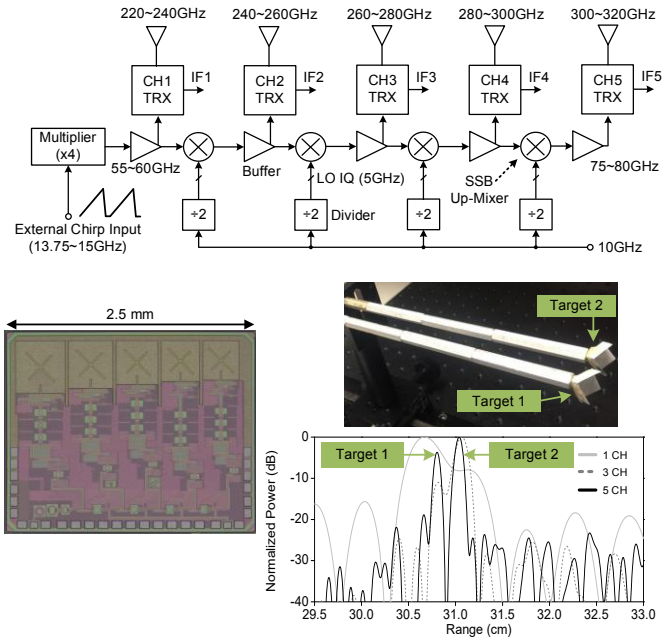

Fig. 4. A 220-to-320GHz CMOS radar transceiver using a frequency comb architecture and delivering <2mm ranging resolution [14].

pairing with a large-aperture lens and provides up to 33dB of TX-RX isolation [13]. With all the above THz CMOS technologies, we see a highly feasible path towards a low-cost imaging radar that offers ultra-high angular resolution and long-distance sensing capability.

Lastly, adopting a THz wave can enable not only high angular resolution, but also high ranging resolution due to the large available bandwidth of the wave. In [14], we present a 220-to-320GHz radar transceiver in CMOS using a frequency comb architecture (Fig. 4). In a conventional, single-tone FMCW radar, an ultra-wide tunable range causes severe performance degradation at the two edges of the band. The comb architecture uses dedicated sub-transceivers to cover narrower sub-bands or channels, hence mitigating the above problem. By "stitching" the IF time-domain signals from all channels, an equivalent broadband FMCW scanning is obtained. In the experiments, this radar exhibits reduced P_{out} and *NF* fluctuation across the 100GHz bandwidth, and effectively resolves two targets spaced by only 2mm in the longitudinal direction.

THz Spectroscopy: From an Electronic Nose to a Clock

The rotational energy of polar gas molecules is quantized to many levels, and to excite quantum transitions among these levels, the required photon frequency could span from the microwave band all the way to far-infrared. Although rotational spectroscopy is not unique in the THz band, for many molecules, two competing factors--the more degenerated sub-states at higher frequency and larger energy-occupation probability (i.e. Boltzmann distribution) at lower frequency, lead to the maximum spectroscopic absorption intensity in the THz range (Fig. 5). In addition, under a low pressure of ~0.1Torr, the Doppler-limited transition linewidth is only at MHz or sub-MHz level (Fig. 5), enabling, according to [15], *absolute specificity* in the analysis of gas mixtures and making THz rotational spectrometer a powerful tool for chemists.

It is noteworthy that the detection of molecular rotational transitions requires CW frequency tuning with high precision and resolution, as well as mW or below power level to avoid power saturation and line broadening [16]. Those make on-chip THz multiplier chain and synthesizer the ideal technical solution. CMOS/SiGe-based THz rotational spectrometers have been demonstrated since 2014 [2], [17], [18]. Similar to ultra-broadband radars, the tradeoff between performance and tuning range exists in single-tone THz spectrometers as well. In addition, spectral scanning with kHz-level resolution across up to 100GHz bandwidth (desired for wide molecule detection range [2]) also takes long time. In [2], the comb

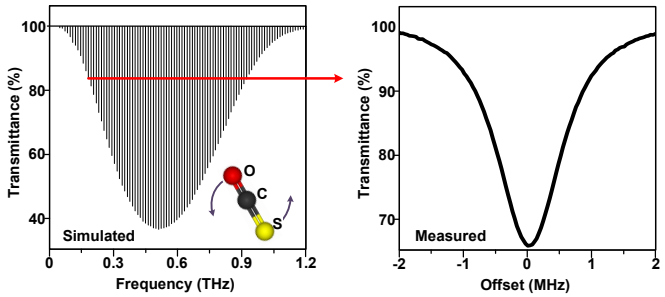

Fig. 5. Rotational transition lines of carbonyl sulfide (OCS) and a measured line profile near 231.061GHz [16], [23].

architecture used in the radar in Fig. 4 is also adopted for a 220-to-320GHz CMOS spectrometer. 10 transceivers are inter-locked and each covers a much narrower sub-band. In the gas detection setup, a pair of these spectrometers are deployed on the two sides of the gas chamber. Driven with a small constant frequency offset, they utilize 20 signal tones to simultaneously probe and scan different parts of the spectrum, which increases the overall scanning speed. The obtained spectral fingerprints of gas mixtures precisely match the existing databases such as the JPL HITRAN.

At present, whether we can develop a highly portable "electronic nose" capable of analyzing complicated gas mixture for applications such as health monitoring through VOC (volatile organic compound) detections remains questionable. As mentioned before, to avoid overlap of the possibly closely-spaced transitions lines from the numerous species, 0.1Torr-level gas pressure is needed. Such pressure level, however, is not readily available from commercial mini pumps. Pre-concentrator of the gas sample also is likely needed to achieve *ppb*-level detection sensitivity. These, rather than the THz electronic hardware, will eventually limit the size and cost of the whole system. On the other hand, for a fair comparison with other gas detection technologies, the vacuum pump should really be viewed as an "*opportunity*" of achieving absolute specificity (not offered by other systems), rather than a fundamental technological *drawback*. The linewidth is roughly proportional to the gas pressure, so even at an easily obtainable pressure level of ~10 Torr, the linewidth is still only ~100MHz (or *Q* of a few thousands); such "sharpness" is still competitive compared to spectrometers operating in other modalities and could be useful for analyzing relatively simple gas compositions. Lastly, we also note that many molecules have redundant transition lines like that in Fig. 5, which means that if line overlap of two different species occur at one frequency, the spectrometer could still examine other line locations and identify the species. Integrating such sensing intelligence, as a good tradeoff for higher gas pressure and smaller system size, could be another strength in using CMOS chips.

While the practicality of THz CMOS spectrometers utilized in gas analytics is still not fully certain, their application in high-precision timing devices, which does not require vacuum pump, pre-concentrator, etc., opens up a new promising direction. As Fig. 5 shows, the Doppler-limited transition line has a *Q* of larger than 10^5. Our analysis and experimental studies also show that the sub-THz transition line of our selected molecule, carbonyl sulfide (OCS), possesses extraordinary frequency stability under temperature change and electrical/ magnetic-field disturbance [19]. It therefore can serve as a high-quality frequency/timing reference. More importantly, this frequency can now be extracted using a THz CMOS spectrometer, enabling clocks with low cost and size. This area has been previously dominated by chip-scale atomic clocks (CSACs) [20], which performs optical-assisted probing of the electron spin resonance near 9.192GHz. With bottle-cap size and ~100mW of DC power, CSACs deliver excellent long-term stability of 10^{-11} or better. They, however, rely on high-precision VCSEL laser and other advanced electro-optical packages, which lead to very high clock cost. The emerging needs for high-stability references, such as the sub μs-level timing synchronization of wireless base stations for 5G and beyond [21], strongly favor clocks with much lower cost.

The above concept, named chip-scale molecular clock by our team at MIT, was first discussed in [16], along with both a tabletop and a

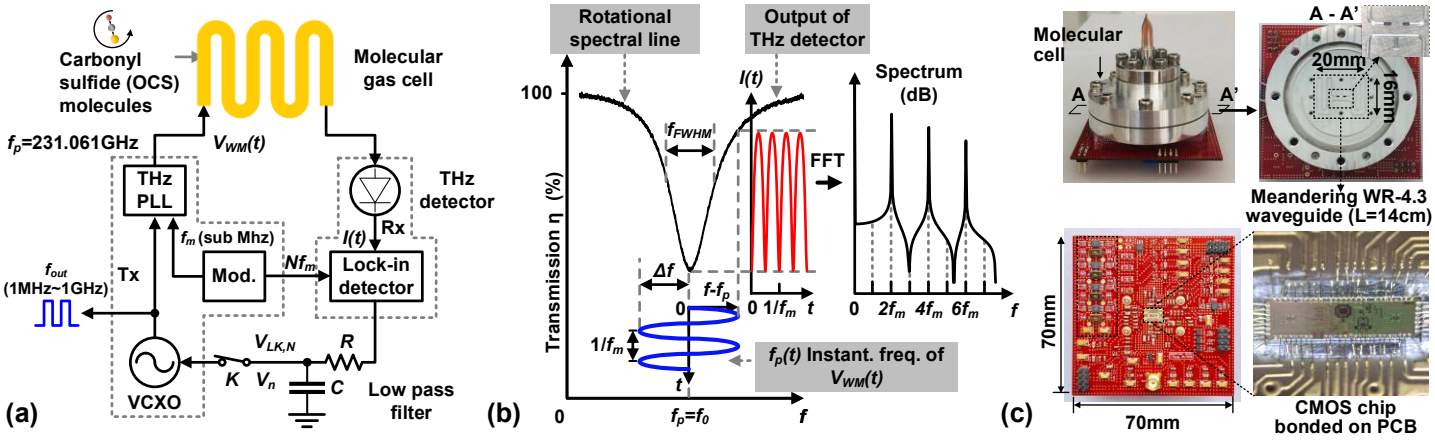

Fig. 6. Chip-scale molecular clock: (a) basic block diagram, (b) spectral line probing based on wavelength modulation, and (c) a CMOS-based prototype [22].

CMOS-based prototypes. The basic block diagram and operation principles of the clock is shown in Fig. 6. Low-pressure OCS gas is hermetically sealed inside a sub-THz single-mode hollow waveguide, in which a probing wave near 231.061GHz is coupled in and out through RF-transparent epoxy windows at the two ends of the waveguide. The probing signal is generated by a Σ-Δ CMOS phase-locked loop (PLL) and is eventually received by an on-chip THz square-law detector. To dynamically align the probing signal at the center of the OCS transition line, its instantaneous frequency $f_p(t)$ is modulated at a sub-MHz rate (f_m) and with a maximum amplitude Δf close to the OCS linewidth. The THz detector output $I(t)$, therefore, responds to the fluctuation of the transmitted signal power. In particular, the amplitude and phase of $I(t)$ at the odd-order harmonics of f_m are used as the error signal to feed back to a voltage-controlled crystal oscillator (VCXO) that drives the THz PLL. This way a frequency-locked loop is formed, which links the MHz VCXO output with the sub-THz OCS transition frequency through a known multiplication factor. The short- and mid-term stability of the clock, quantified by Allan deviation, is determined by the *Q* of the transition line and the *SNR* of the chip-measured line curve. In our clock, the CMOS spectrometer generates a very smooth transition line curve, with a *SNR* of 84dB [22].

Our development of the molecular clock have gone through three generations [22]–[24]. The most recent prototype [24], with a size similar to that of a CSAC, consumes 71mW of power. Without relying on any ovenized temperature regulation and post temperature compensation—both adopted in CSACs, the measured temperature coefficient of the clock is 5.8×10^{-10}/ºC over -20~60ºC range. The Allan Deviation achieved by the clock is 2×10^{-11} with 10,000s averaging time, and should go below 10^{-11} when active thermal regulation and/or post temperature compensation is applied. Such stability performance is already very similar to that of state-of-the-art CSACs. At present, the gas cell of the clock is made from a CNC-machined aluminum waveguide. That could be eventually replaced by MEMS-based miniature waveguides in silicon. Such waveguides have already been reported [25], with measured insertion loss lower than that of the CNC-based waveguides. Although more research is needed regarding the hermetic sealing technique and performance, this could be a very promising approach to further improve the molecular clock's stability performance and reduce the size to under $1cm^3$.

THz Communication: What Can We Do Besides Ultra-High-Speed Wireless?

While ultra-high-speed wireless remains an important application for THz CMOS circuits, the transistor performance and the implemented beam-forming array scale probably should gain much more improvement in order to obtain sufficient link budget to enable truly practical Tbps wireless systems. Before this happens, what else can we do in the field of THz communications?

First, THz communication can be applied to >100Gbps *wireline* applications. The concept of "radio-over-fiber" has been pursued as a promising alternative to copper electrical links and fiber optic links, especially for meter-class, high density interconnection scenarios. For ultra-broadband transmission, dielectric waveguides offer much lower signal loss and dispersion compared to copper cables, which should save significant power from cable drivers and equalizers. Compared to photonic links, the radio-over-fiber scheme is capable of connecting two standard silicon chips together, which offers better hardware compatibility. The choice of carrier frequency in a dielectric waveguide link is largely determined by the application. Higher frequency allows for shorter transmission distance, but the larger available bandwidth enables higher data rate. And since the width of the waveguide is proportional to the wavelength, higher carrier frequency also increases the link data rate density (Gbps/mm). In [26], MIT and Intel present a 220-to-320GHz dielectric waveguide link using a 130nm BiCMOS process. The TX of the link is shown in Fig. 7, where three carriers at 220, 260 and 300GHz are generated using a comb architecture, and then BPSK-modulated by three 35Gbps data streams respectively. Through an on-chip triplexer and an on-chip substrate-integrated-waveguide (SIW) coupler [27], the three channels are aggregated and launched into a single-mode dielectric waveguide. The waveguide has a cross-sectional area of only 400x250μm^2, which corresponds to 332Gbps/mm link density. On the receiver side, each channel is de-modulated by a double-balanced THz mixer. 105Gbps data transmission over 30cm distance is demonstrated, and the energy efficiency including only the mmWave/THz front-ends is 2.4pJ/b for TX and 2.1pJ/b for RX. If using higher-order modulation scheme and multiple electromagnetic modes in the waveguide, it is possible that the data rate is further increased to 200Gbps or even 400Gbps. In the future, more R&D work should also be done for the dielectric waveguide, in order to achieve lower insertion loss, higher robustness against touching and

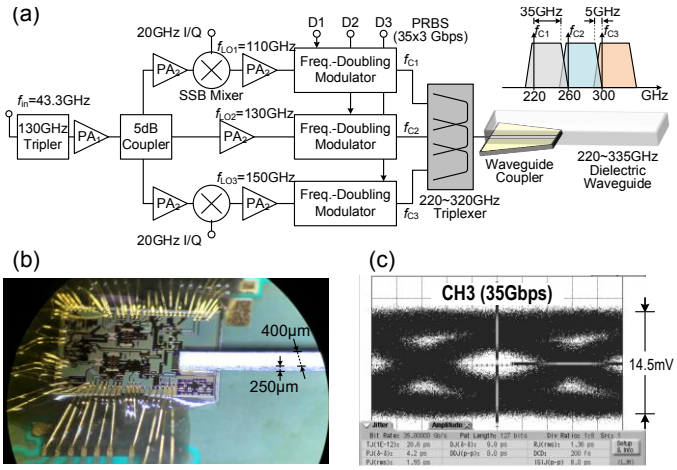

Fig. 7. A 105Gbps dielectric waveguide link [26]: (a) block diagram of the transmitter, (b) die photo of the transmitter, and (c) measured eye diagram of the third channel.

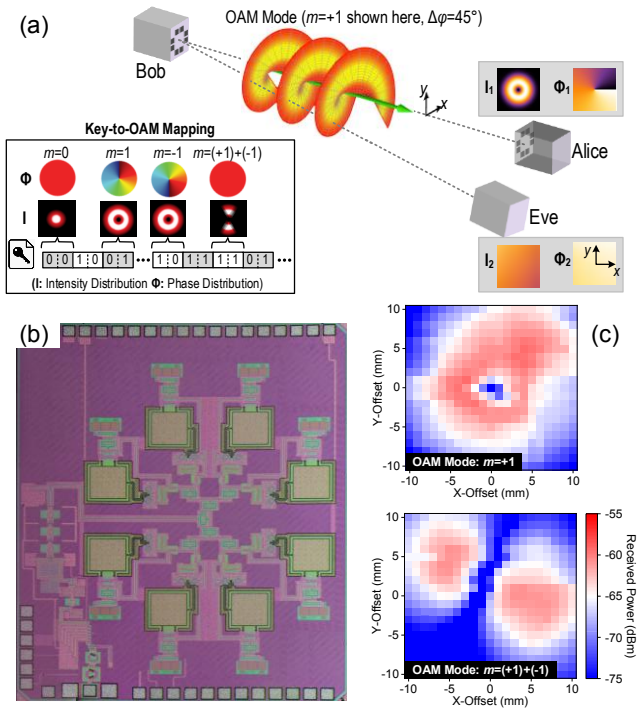

Fig. 8. CMOS THz OAM transceiver [28]: (a) application in alignment-sensitive security key transmission, (b) die photo and (c) measured wavefront intensity at different OAM modes.

bending of the waveguides, as well as suitable connectors between the waveguide and the chip.

It is noteworthy that, although the link budget provided by current CMOS THz chips still face challenges in meeting the need of high-speed wireless transmission, it could still be sufficient for Mbps-level data rate. For most applications, such slow wireless links simply do not make sense; but if it is only used for the transmission of an encryption key (e.g. AES security key), which is typically only 128bit or 256bit long, it could still be practical, as long as additional physical-layer security is provided. In [28], Han's and Chandrakasan's teams at MIT explored this direction using the transmission of THz waves with orbital angular momentum (OAM). An OAM wave possesses a wavefront with twisted phase distribution around the axis of the propagation (Fig. 8). Different twist directions (left-handed or right-handed) and total phase change per twist ($2m\pi$, where m=0,±1,±2…) correspond to different OAM modes. In our proposed transmission protocol in Fig. 8a, the values of digits in a security key can be mapped to different OAM modes. To identify the mode of the OAM wave, the receiver should be able to compare the phases of multiple parts of the incoming wavefront around the propagation axis. That is only possible when the receiver (Alice in Fig. 8) is precisely located at the axis. For an off-axis eavesdropper (Eve in Fig. 8), the quality of the above phase comparison drops rapidly with the misalignment angle. Given the large phase noise of the THz signal, that leads to a very narrow angular space in which the detection of the OAM modes (hence the bits of the key) can be successful [29].

Before this study, there was no report of on-chip OAM transmitters/receivers at any frequency. In [28], the MIT team for the first time present a CMOS transceiver dealing with OAM waves at 310GHz. Shown in Fig. 8b, the chip has 8 patch antennas driven through certain phase combinations and supports wave modes of m=0 (plane wave), m=+1 (left-handed), m=-1 (right-handed) and m=(+1)+(-1) (superposition). In the experiments, the output OAM modes are verified through 3D-printed spiral phase plates and the scanning of the wavefront profiles (Fig. 8c). The chips also successful demonstrated our proposed key-to-OAM wireless data transmission with a measured data rate of 1Mbps and high sensitivity to the TX-RX co-axial alignment.

THz-ID: mm-Sized Tag with Backscatter Communications

Operating at the THz frequencies allows for shrinking size of the antenna and directly integrating it on the chip. This feature could be highly attractive to systems where antenna limits the size and even the cost. RF identification (RFID) tags are such cases: although the RFID silicon chip itself is small, the whole tag still relies on a cm-scale external antenna or inductor for the far-field or near-field electromagnetic power coupling at MHz frequencies. That makes it impossible to directly attach the tag to objects such as medical pills, tooth implants and semiconductor chips, etc., for authentication and logistical tracking. In [30], a THz-ID technology is introduced by Han and Chandrakasan's team at MIT, which utilizes 260GHz carriers for downlink and backscatter-communication-based uplink. As a result, within a 1.2×1.3mm^2 CMOS chip area, a 2x2 patch antenna array is integrated, leading to a packageless tag. For the downlink, four THz square-law detectors cascaded by an ultra-low-power amplifier are used. For the uplink, a cross-polarization scheme similar to that in the reflectarray work described earlier [11] is adopted: the incident wave power is extracted differentially from a patch edge and then injected into a single-sideband frequency mixer. The mixer shifts the frequency of the THz signal by f_{LO}~2MHz and then re-feeds it back to the center of the same patch edge, which excites the radiation with a polarization orthogonal to that of the input. The uplink data modulation is done through an ASK switching of the 2MHz LO signal of the mixer. The cross-polarization and frequency-duplexing adopted in the uplink ensures that the small-power, backscattered signal is not masked by the high phase noise of any incident carrier wave that is directly reflected by the surface of the tagged object. The ID chip is powered by an on-chip photodiode array. A fishnet pattern is created in each on-chip patch antenna to allow light illumination on photodiodes under the antenna. In our simulation, a 25% fill factor of light windows on the antenna only reduces the radiation efficiency from 31% to 27%. To ensure that the THz-ID only responds to legitimate readers, the chip is also equipped with an ultra-low-power elliptic-curve-cryptographic (ECC) processor, which offers high security asymmetric encryption. The chip consumes 21μW of DC power, most of which is for the on-chip cryptographic

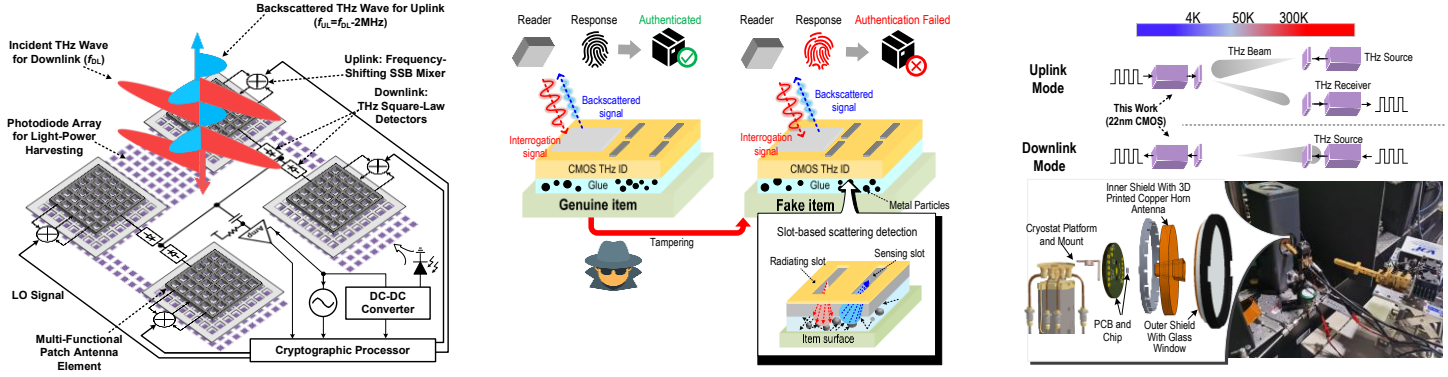

(a) Cryptographic THz-ID (b) Anti-Tampering Tag (c) 4Gbps Cryogenic Backscatter Link

Fig. 9. Backscatter-communication-based, miniature THz platforms for (a) cryptographic [30] and (b) anti-tampering [32] ID tags, and (c) wireless up/down links in a 4K cryostat [34].

processor. In our experiment, 100kbps downlink speed and 2kbps uplink speed are demonstrated, with a 5-cm reader-ID interrogation distance. Through the on-chip 2x2 antenna array, we also demonstrate that, when the THz-ID does not face the reader in the perpendicular direction, it can steer its backscatter power towards the reader in order to maximize the link budget. This capability was not possible in prior single-antenna/inductor RFIDs.

The above THz-ID relies on photovoltaic powering, which could limit its applications in, for example, opaque object packages. It would be ideal if the incident THz carrier can be directly converted to DC power. To that end, we implemented the first CMOS-based THz energy harvester in [31], using Intel-16 FinFET technology. Using a dual-antenna-feed architecture and a self-gate-biasing scheme, the optimal transistor rectification condition is achieved. Under -8dBm input power, which matches that in the THz-ID reader interrogation scenario, the harvester delivers 22μW of DC power and an RF-to-DC conversion efficiency of 13.6%. This work demonstrates the feasibility of a packageless THz-ID that can be entirely powered through the THz carrier wave, which is more convenient to use.

Although the THz-ID was intended to authenticate commercial goods, one security loophole exists. If the tag is detached from a genuine item and re-attached onto a counterfeit item, such tampering cannot be detected. To fix this problem, in [32], an anti-tampering tag is presented by the Han and Chandrakasan's teams at MIT. Shown in Fig. 9b, the glue used for attaching the chip tag onto the object contains metal particles; the sizes and spatial distribution of the particles are random. They are also automatically altered when the tag is detached, and therefore can serve as a physically unclonable fingerprint for authentication integrity. In Fig. 9b, the sub-THz interrogation signal from the reader, after received by the tag, gets further radiated onto the interface between the CMOS chip and the object surface. The wave is then scattered by the metal particles and other textures of the interface, and is sent back to the chip and then further transmitted to the reader. As a result, the transfer function between the reader's outgoing and return signals, as well as its variations at different frequencies, can be used to determine if the above fingerprint is altered or not. In [32], a trained Siamese neural network is adopted to achieve 99.34% accuracy for the above tampering-identification process.

The miniaturization approach using THz carrier can also be applied to other RF systems. For example, in [33], a 1.54mm^2 CMOS wake-up receiver operating with 260GHz carrier is demonstrated. Pairing with the reflectarray system described earlier in this paper, it can be activated by the steered beam across multi-meter distance. The work may be applied to save power in ultra-small, micro-battery-powered platforms such as non-intrusive sensor nodes and micro-robots. Lastly, the THz backscatter communication adopted in the THz-IDs can also enable very novel applications in other fields. In [34], the Han and Englund's teams at MIT use this technology to address the large heat load problems of 4-Kevin cryogenic facilities. At present, metallic cables are used to transport data between the 300-Kevin and 4-Kevin environment. They, however, pose high heat load (>1mW/cable) to the cryostat and reduce the allowable power consumption inside. By adopting a THz-ID-like CMOS chip inside the cryostat, the downlink and uplink are achieved wirelessly through the cryostat glass window, hence cutting the thermal conduction path. Interestingly, both the on-chip antenna radiation efficiency and the MOSET nonlinearity used for THz square-law detection are increased significantly under 4K, which lead to high energy efficiency. In the experiment, the downlink and uplink achieve 4Gbps data rate and energy efficiency of 34fJ/b and 176fJ/b, respectively, which show the potential of deploying this THz-based scheme in future cryogenic hardware.

Conclusions

The combination of CMOS and THz technologies not just improves the practicality of the existing THz applications and systems. More importantly, the studies presented in this paper show that, operating at THz frequencies could also offer effective approaches that dramatically improves the electronics for traditional applications, such as radar sensing, timing, wireline interconnects, security and RF tagging. Further investigation into this research domain will greatly incentivize the commercialization and wide adoption of THz CMOS integrated circuits.

Acknowledgement:

The author thanks all the contributors to the research works described in this paper, especially the prior and current members of his research group at MIT: Nathan Monroe, Xibi Chen, Xiang Yi, Cheng Wang, Mina Kim, Jack Holloway, Muhammad Khan, Mohammad Ibrahim, Zhi Hu, Eunseok Lee and Jinchen Wang. The author also thanks his collaborators, Prof. A. Chandrakasan (MIT), Prof. D. Englund (MIT), Prof. H. Lee (MIT), Dr. George Dogiamis (Intel), Dr. Lin Yi (NASA JPL), Dr. K. Kolodziej and Dr. Brad Perkins (MIT Lincoln Labs). These works are sponsored by NSF, Intel, ONR, ADI, MIT Lincoln Labs, MIT SMART program, TSMC, TI, ADI, Mitsubishi Electric, Naval Research Labs, TDK USA and Azbil.

References:

[1] E. Seok *et al.*, "A 410GHz CMOS Push-Push Oscillator with an On-Chip Patch Antenna," in *International Solid-State Circuit Conference (ISSCC)*, San Francisco, 2008.

[2] C. Wang and R. Han, "Dual-Terahertz-Comb Spectrometer on CMOS for Rapid, Wide-Range Gas Detection with Absolute Specificity," *IEEE J Solid-State Circuits*, vol. 52, no. 12, pp. 3361–3372, 2017.

[3] K. Takano *et al.*, "A 105Gb/s 300GHz CMOS transmitter," *IEEE International Solid-State Circuits Conference*. San Francisco, CA, 2017.

[4] P. Rodriguez-Vazquez, J. Grzyb, B. Heinemann, and U. R. Pfeiffer, "A QPSK 110-Gb/s Polarization-Diversity MIMO Wireless Link with a 220-255 GHz Tunable LO in a SiGe HBT Technology," *IEEE Trans Microw Theory Tech*, vol. 68, no. 9, pp. 3834–3851, Sep. 2020.

[5] C. M. Armstrong, "The Truth About Terahertz," *IEEE Spectr*, vol. 49, no. 9, pp. 36–41, 2012.

[6] R. Al Hadi *et al.*, "A 1 k-pixel video camera for 0.7-1.1 terahertz imaging applications in 65-nm CMOS," *IEEE J Solid-State Circuits*, vol. 47, no. 12, pp. 2999–3012, 2012.

[7] K. Su, L. Moeller, R. B. Barat, and J. F. Federici, "Experimental comparison of terahertz and infrared data signal attenuation in dust clouds," *Journal of the Optical Society of America A*, vol. 29, no. 11, pp. 2360–2366, 2012.

[8] K. Su, L. Moeller, R. B. Barat, and J. F. Federici, "Experimental comparison of performance degradation from terahertz and infrared wireless links in fog," *Journal of the Optical Society of America A*, vol. 29, no. 2, p. 179, 2012.

[9] J. Ma, F. Vorrius, L. Lamb, L. Moeller, and J. F. Federici, "Experimental Comparison of Terahertz and Infrared Signaling in Laboratory-Controlled Rain," *J Infrared Millim Terahertz Waves*, vol. 36, no. 9, pp. 856–865, 2015.

[10] "Atmospheric Attenuation at THz," *Virginia Diode Inc. Application Note*.

[11] N. M. Monroe, G. C. Dogiamis, R. Stingel, P. Myers, X. Chen, and R. Han, "Electronic THz Pencil Beam Forming and 2D Steering for High Angular-Resolution Operation: A 98x98 Unit 265GHz CMOS Reflectarray with In-Unit Digital Beam Shaping and Squint Correction," in *IEEE International Solid-State Circuits Conference (ISSCC)*, San Francisco, CA, 2022, pp. 51–53.

[12] J. W. Holloway, G. C. Dogiamis, S. Shin, and R. Han, "220-to-330-GHz Manifold Triplexer With Wide Stopband Utilizing Ridged Substrate Integrated Waveguides," *IEEE Transactions on Microwave Theory and Techniques (T-MTT)*, vol. 68, no. 8, pp. 3428–3438, 2020.

[13] X. Chen *et al.*, "A 140GHz Transceiver with Integrated Antenna, Inherent-Low-Loss Duplexing and Adaptive Self-Interference Cancellation for FMCW Monostatic Radar," *IEEE J Solid-State Circuits*, *ISSCC Special Issue*, vol. 57, no. 12, pp. 3631–3645, 2022.

[14] X. Yi, C. Wang, X. Chen, J. Wang, J. Grajal, and R. Han, "A 220-to-320-GHz FMCW Radar in 65-nm CMOS Using a

Frequency-Comb Architecture," *IEEE J Solid-State Circuits-ISSCC Special Issue*, vol. 56, no. 2, pp. 327–339, 2021.

[15] I. R. Medvedev, C. F. Neese, G. M. Plummer, and F. C. De Lucia, "Submillimeter Spectroscopy for Chemical Analysis with Absolute Specificity," *Opt Lett*, vol. 35, no. 10, pp. 1533–5, 2010.

[16] C. Wang, X. Yi, J. Mawdsley, M. Kim, Z. Wang, and R. Han, "An On-Chip Fully-Electronic Molecular Clock Based on sub-THz Rotational Spectroscopy," *Nat Electron*, vol. 1, no. 7, pp. 421–427, 2018.

[17] K. Schmalz, R. Wang, Y. Mao, W. Debski, and H. Gulan, "245 GHz SiGe Sensor System for Gas Spectroscopy," pp. 644–647, 2014.

[18] Q. Zhong, W. Choi, C. Miller, R. Henderson, and K. K. O, "A 210-to-305GHz CMOS receiver for rotational spectroscopy," in *2016 IEEE International Solid-State Circuits Conference (ISSCC)*, San Francisco, CA, 2016.

[19] M. Kim, C. Wang, Z. Hu, and R. Han, "Chip-Scale Terahertz Carbonyl Sulfide (OCS) Clock : An Overview and Recent Studies on Long-Term Frequency Stability of OCS Transitions," *IEEE Trans Terahertz Sci Technol*, 2019.

[20] R. Lutwak, "Principles of Atomic Clocks," in *IEEE International Frequency Control Symposium*, San Francisco, CA, 2011.

[21] H. Li, L. Han, R. Duan, and G. M. Garner, "Analysis of the Synchronization Requirements of 5G and Corresponding Solutions," *IEEE Communications Standards Magazine*, vol. 1, no. March, pp. 52–58, 2017.

[22] C. Wang, X. Yi, M. Kim, Q. Ben Yang, and R. Han, "A Terahertz Molecular Clock on CMOS Using High-Harmonic-Order Interrogation of Rotational Transition for Medium-/Long-Term Stability Enhancement," *IEEE J Solid-State Circuits-ISSCC Special Issue*, vol. 56, no. 2, pp. 566–580, Feb. 2021.

[23] C. Wang *et al.*, "Chip-Scale Molecular Clock," *IEEE J Solid-State Circuits*, vol. 54, no. 4, 2019.

[24] M. Kim, C. Wang, L. Yi, H. S. Lee, and R. Han, "A Sub-THz CMOS Molecular Clock with 20 ppt Stability at 10,000 s Based on Dual-Loop Spectroscopic Detection and Digital Frequency Error Integration," in *Digest of Papers - IEEE Radio Frequency Integrated Circuits Symposium*, Institute of Electrical and Electronics Engineers Inc., 2022, pp. 115–118.

[25] B. Beuerle, J. Campion, U. Shah, and J. Oberhammer, "A Very Low Loss 220-325 GHz Silicon Micromachined Waveguide Technology," *IEEE Trans Terahertz Sci Technol*, vol. 8, no. 2, pp. 248–250, 2018.

[26] J. W. Holloway, G. C. Dogiamis, and R. Han, "A 105Gb/s Dielectric-Waveguide Link in 130nm BiCMOS Using Channelized 220-to-335GHz Signal and Integrated Waveguide Coupler," in *IEEE International Solid-State Circuits Conference (ISSCC)*, San Francisco, CA, 2021, pp. 27–28.

[27] J. W. Holloway, L. Boglione, T. M. Hancock, and R. Han, "A Fully Integrated Broadband Sub-mmWave Chip-to-Chip Interconnect," *IEEE Trans Microw Theory Tech*, vol. 65, no. 7, 2017.

[28] M. I. W. Khan *et al.*, "A 0.31-THz Orbital-Angular-Momentum (OAM) Wave Transceiver in CMOS with Bits-to-OAM Mode Mapping," *IEEE J Solid-State Circuits*, vol. 57, no. 5, pp. 1344–1357, May 2022.

[29] J. Woo, M. I. Wasiq Khan, M. I. Ibrahim, R. Han, A. P. Chandrakasan, and R. T. Yazicigil, "Physical-Layer Security for THz Communications via Orbital Angular Momentum Waves," in *IEEE Workshop on Signal Processing Systems, SiPS: Design and Implementation*, Institute of Electrical and Electronics Engineers Inc., 2022.

[30] M. I. W. Khan *et al.*, "CMOS THz-ID: A 1.6-mm^{2}Package-Less Identification Tag Using Asymmetric Cryptography and 260-GHz Far-Field Backscatter Communication," *IEEE J Solid-State Circuits-ISSCC Special Issue*, vol. 56, no. 2, 2021.

[31] M. Ibrahim Wasiq Khan, E. Lee, N. M. Monroe, A. P. Chandrakasan, and R. Han, "A Dual-Antenna, 263-GHz Energy Harvester in CMOS for Ultra-Miniaturized Platforms with 13.6% RF-to-DC Conversion Efficiency at -8 dBm Input Power," in *IEEE Radio-Frequency Integrated Circuit Symposium (RFIC)*, 2022.

[32] E. Lee, X. Chen, M. Ashok, J. Won, A. Chandrakasan, and R. Han, "A Packageless Anti-Tampering Tag Utilizing Unclonable Sub-THz Wave Scattering at the Chip-Item Interface," in *IEEE International Solid-State Circuits Conference (ISSCC)*, 2024.

[33] E. Lee *et al.*, "A 1.54mm2 Wake-Up Receiver Based on THz Carrier Wave and Integrated Cryptographic Authentication," in *Proceedings of the Custom Integrated Circuits Conference*, Institute of Electrical and Electronics Engineers Inc., 2023.

[34] J. Wang *et al.*, "THz Cryo-CMOS Backscatter Transceiver: A Contactless 4 Kelvin-300 Kelvin Data Interface," in *Digest of Technical Papers - IEEE International Solid-State Circuits Conference*, 2023, pp. 504–506.